Anal. Bioanal. Electrochem., Vol. 10, No. 4, 2018, 508-519

Analytical & Bioanalytical Electrochemistry

2018 by CEE
www.abechem.com

Full Paper

Polyvinylpyridine (PVP)-grafted Magnetite Nanoparticles: Facile Fabrication through Cathodic Deposition from Ethanol Media and their Physico-Chemical Properties

Mustafa Aghazadeh

Materials and Nuclear Research School, Nuclear Science and Technology Research Institute (NSTRI), P.O. Box 14395-834, Tehran, Iran

*Corresponding Author, Tel.: +98-21-82064289; Fax: +98-21-82064289

E-Mail: maghazadeh@aeoi.org.ir

Received: 23 February 2018 / Accepted: 15 April 2018 / Published online: 30 April 2018

Abstract- Pristine crystalline superparamagnetic nanoparticles (SPNs) of magnetite (Fe_3O_4) were prepared from an additive-free aqueous solution of iron(III) nitrate salt *though* a novel one-pot electrodeposition method. The prepared nanoparticles were characterized by XRD, IR, VSM, DLS and FE-SEM. The SPNs were further grafted by poly(N-vinyl-2-pyrrolidone) during their deposition process. The PVP-grafting via electrochemical route was confirmed by IR, DSC-TGA and DLS analyses. The analyses results confirmed the proper phase (i.e. pristine magnetite), size (about 10 nm) and excellent super-paramagnetic nature (*Ms=48.57*emu g^{-1}, *Mr*≈0.038 emu g^{-1} and *Ce*~1.35*G*) of the prepared PVP-grafted Fe_3O_4 nanoparticles for biomedical applications.

Keywords- Iron oxide, Magnetic properties, Nanoparticles, Electro-chemical deposition, PVP grafting, Biomaterials

1. INTRODUCTION

The superparamagnetic iron oxide nanoparticles (SPNs) have been subject of many investigations because of their promising uses as hyperthermia, drug delivery, cell separation and MRI [1-4]. Up now, various techniques for the preparation of soluble or insoluble SPIONs have been constructed, which include co-precipitation [5-7], synthesis in reverse micelles [8], sonolysis [9], electrochemical deposition [10-12], mechanochemical dispersion

[13], solution plasma [14], sol–gel processes [15], arc discharge [16], spray [17], pyrolysis [18], thermal decomposition [19,20], hydrothermal [21-23], solvothermal [24] and combustion synthesis [25,26]. In terms of the advantages and disadvantages for preparing iron oxide nanoparticles (IONPs), regarding their size and morphology control, thermal decomposition and hydrothermal synthetic routes have mentioned to be the optimal method [19-23]. Furthermore, for obtaining water-soluble and biocompatible SPIONs, co-precipitation is often employed, but this method presents low control of the particle shape, and can result in a broad distribution of sizes and aggregation of the particles [6,7]. Also, as a time-competitive alternative, the sonochemical route has been introduced to synthesize iron oxide NPs, however, the prepared SPNs usually represent unusual magnetic properties. Reviewing the results of the reports about preparation of SPIONs synthesis reveals that although the various above mentioned methods have been modified in the recent years, however controlling the magnetite particle size and distribution, and magnetic properties are the unsolved problems in this area. In this regard, we recently developed cathodic electrochemical deposition (CED) technique as facile and fast route for fabrication of bare and coated SPIONs [27-30]. Notably, cathodic electrodeposition represents simple and effective way for the preparation of nanoparticles of metal oxides and hydroxides [31-43]. Furthermore, the anodic electrodeposition has been also reported for the synthesis of bare SPNs [44-51], where this deposition platform has limitations of high voltage values (40-62 V), critical distance between anode and cathode (<5 cm), as well as the presence of supporting electrolytes and/or surfactants [46-48,51]. Recently, we found that cathodic deposition refines limitations of anodic deposition route [52-55] and exhibits versatile route for deposition of magnetite NPs. In the synthesis of iron oxide, poly(vinylpyrrolidone) (PVP)has been used as stabilizer and coating agent to fabricate ultra-small SPNs through the co-precipitation, hydrothermal and thermal decomposition methods [56-60]. It was found that pyrrolidone functional groups of PVP molecules can easily arrest crystals of SPIONs with helping to form ultrafine magnetic particles and preventing the aggregation of the nanoparticles. For example, Lee et al. [56] prepared PVP-coated iron oxide nanoparticles by the thermal decomposition of $Fe(CO)_5$ and confirmed their biocompatibility in MRI studies. Zheng *et al.* [57] fabricated ultra-small magnetite NPs through co-precipitation method in the presence of PVP as a stabilizer. They found that PVP molecules not only prevent the aggregation of the Fe_3O_4 nanoparticles, but also restrict their size by utilizing the interaction between the carbon atoms in carbonyl groups and the Fe atoms on the magnetite NPs. Lee *et al.* [58] reported the thermal decomposition route for synthesis of biocompatible PVP-grafted iron oxide NPs and evaluation of their efficacy as a MRI contrast agent. Lu and co-workers synthesized magnetite nano-crystals using pyrolysis of iron(III) acetate in N-vinyl-2-pyrrolidone, which was polymerized in-situ to PVP [60]. Based on the above explanations, the current work deals with the development of facile deposition platform of pristine and

poly(vinylpyrrolidone) (PVP) grafted SPNs form iron nitrate dissolved ethanol (96%) electrolyte. To the best of our knowledge, the electrosynthesis of PVP grafted SPNs from ethanol medium, has not been reported up now. The prepared sample was characterized using various analyses of XRD, IR, VSM, TG and FE-SEM, and the results proved the successful one-step electrochemical preparation of PVP-grafted SPINs from ethanol electrolyte.

2. EXPERIMENTAL PROCEDURE

2.1. Materials

Iron(III) nitrate ($Fe(NO_3)_2.9H_2O$, 99.95%) and poly(vinylpyrrolidone) (PVP, Mw=4000) were purchased from Sigma-Aldrich.

2.2. Electrosynthesis of pristine magnetite nanoparticles

Pristine nanoparticles of magnetite were prepared *through* our recently developed cathodic electro-synthesis (CES) strategy [52,61]. Here, the electrolyte-type and iron salt were changes as compared with previous reports [56,59]. The ethanol (96%) and only Fe(III) nitrate were chosen as the electrolyte for deposition of iron oxide (as shown in Fig. 1a). A stainless-steel cathode centered between two graphite anode was used as two-electrode system. 2.4 g of Fe(III) nitrate salt was dissolved in ethanol (96%) and used as the CES electrolyte. The CE deposition of SPNs was carried out with applying 5 mA cm^{-2} for 30 min(Fig. 1). After, electrodeposition on stainless steel electrode, the purification and separation steps were done as follow; (i) the steel electrode was brought out from the electrolyte and washed for several times and the black deposited film was scraped, (ii) then, the deposit was dissolved in ethanol, (iii) centrifuged at 6000 rpm for 5 min, and (iv) at final step, the deposit was separated from the ethanol solution by the magnet and dried at RT for 4 h. The obtained dry black powder was labeled as pristine magnetite sample, and analyzed through by different characterization techniques.

2.3. Electrosynthesis of PVP grafted magnetite nanoparticles

For the preparation of PVP-grafted SPNs, the same electrochemical set up and material was used as presented in Fig. 1b, i.e. (i) electrochemical workstation system (Potentiostat/Galvanostat, Model: NCF-PGS 2012, Iran), (ii) a two-electrode electrochemical cell stainless-steel cathode, (iii) graphite anode, (iv) 0.005 M $Fe(NO_3)_3$ dissolved in ethanol solution, (v) galvanostatic electrodeposition mode (I=t mA cm^{-2}), (vi) T= 25 ^oC and t=30 min. Only the bath composition was changed with addition of 1 g $L^{-1}$of PVP to the ethanol electrolyte. The PVP-grafted SPNs were prepared under constant current mode for 30 min (Fig. 1b). After the CES procedure, the deposited black film on cathode surface was repeatedly rinsed with ethanol. In the next step, the deposited black film was removed from

the cathode, and dispersed in ethanol (96%) and centrifuged at 3000 rpm for 10 min to remove the weekly bonded polymer to the surface of SPNs. In final step, the dispersed deposited was separated from the solution with magnet (Fig. 1b). Then the fabricated PVP-grafted SPNs were dried in 60 ^{o}C for 1h, and used in characterization analyses.

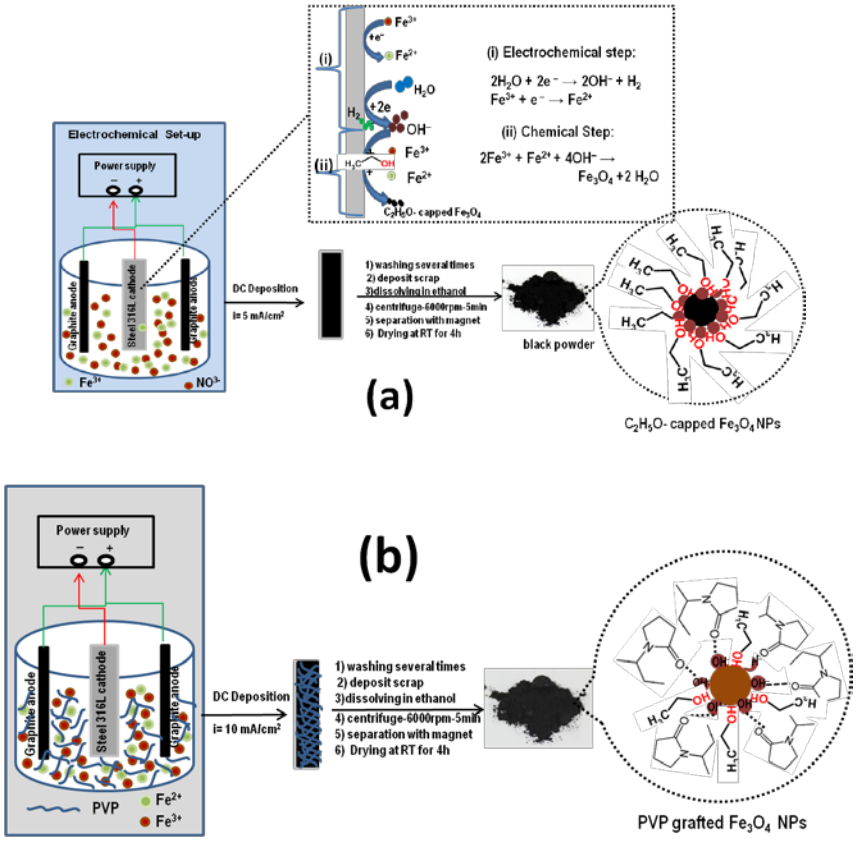

Fig. 1. Formation processes of (a) the pristine and (b) the PVP-grafted SPNs

2.4. Characterization

The prepared NPs were monitored using a Field-emission electron microscopy (FE-SEM, model Mira 3-XMU with an accelerating voltage of 100 kV) to specify the size and shape of the fabricated particles. The crystal phase and structure were determined by XRD, model Phillips PW-1800 diffractometer with Co Kα radiation (λ=1.789 Å)). The hydrodynamic diameter was determined by dynamic light scattering (DLS, 4700 Malvern Instruments, UK). FTIR spectra were recorded using a Bruker Vector 22 Fourier transformed infrared spectroscope. The thermal behavior analyses were carried out in an N_2atmosphere between room temperature and 600 ^{o}C at a heating rate of 5^{o}C min^{-1} using a thermoanalyzer (STA-1500). The magnetic properties of NPs were measured from −20000 to 20000 Oe at room temperature using VSM (Meghnatis Daghigh Kavir Co., Iran).

3. RESULTS AND DISCUSSION

The crystalline properties of the SPNs were analyzed through XRD as shown in Fig. 2. For both samples, all observed peaks were completely in agreement with spinal structure of magnetite (JCPDS card No. 01-088-0315). Using the Debye–Sherrer equation ($D=K\lambda/\beta\cos\theta$), the average crystallite size was calculated to be about 7.4 and 6.2 nm for pristine and PVP-grafted SPNs, respectively.

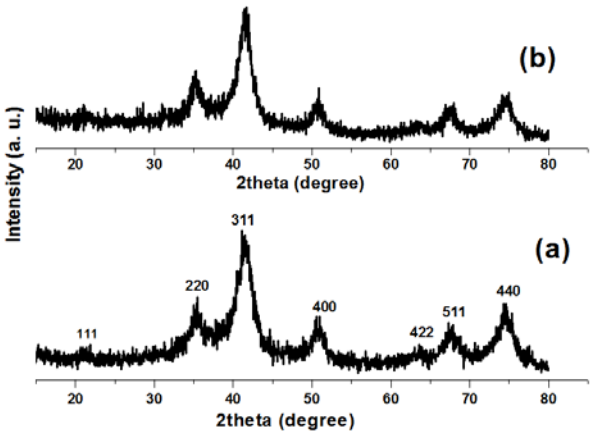

Fig. 2. XRD patterns of (a) the pristine and (b) the PVP-grafted Fe_3O_4 NPs

The IR spectra of both pristine and PVP-grafted magnetite NPs are presented in Fig. 3. In both FTIR spectra (Fig. 3), the broad band at ~3430-50 cm^{-1} is related to the stretch vibration mode of the OH group in water molecules adsorbed on the SPNs surface [54,58]. Also, the IR bands located below 700 cm^{-1} are due to the Fe-O stretch modes [55-56], and confirming the magnetite (i.e. Fe_3O_4) composition of both electro-deposited samples.

The IR spectrum of pristine SPNs in Fig. 3a has extra bands, which included [52]; the peaks of magnetite are observed at 437 and 412 cm^{-1} resulting from a split of the ν_1 band of the Fe—O bond, and two broad bands around 621 and 571 cm^{-1} originating from the ν_2 stretching vibrations of Fe-O bond [29-31]. The absorption bands around 1624 and 3450 cm^{-1} are also due to the stretching and deformation vibrations OH groups attached to the surface of MNPs [52]. Furthermore, several IR vibrations relating to the chemical bonds of CH_2, C-C, C-H and C-O are observed [52], which are as follow; (i) C-C stretching at 1177 cm^{-1}, (ii) CH_3 rock at 1373 cm^{-1}, (iii) CH_2 symmetric vibration at 2876 cm^{-1}, (iv) CH_2 asymmetric vibration at 2979 cm^{-1}, (v) C-O bending at 1021 cm^{-1}, (vi) C-H bending at 926 cm^{-1}, (vii) C-O stretching at 1105 cm^{-1}, and (viii) -CH_2 stretching at 1243 cm^{-1} [52,60,61]. These findings proved the presence of C_2H_5O- groups on the surface of deposited SPNs from ethanol electrolyte, as we reported in previous work [52], and schematically shown in Fig. 1a.

The spectra of the PVP-grafted SPNs has some extra IR bands located at 2924, 2863, 1476, 1349 and 1244 cm^{-1}, which are corresponded to the CH_2 groups vibration modes of

PVP polymer [55,56]. Furthermore, C-N stretching mode at 1297 and 1017 cm^{-1} and C=O group vibration at 1622 cm^{-1} are also seen. It has been reported that the carbonyl group vibration of pristine PVP is located at about 1649 cm^{-1} [57,59]. Hence, the chemical interaction between carbonyl groups and the magnetite NPs is evidenced form the C=O band shift i.e. from 1649 to 1622 cm^{-1}. Furthermore, the ethoxy group vibrations (i.e. CH3, C-O and C-C) are also observable in Fig. 3b. Hence the prepared magnetite NPs in the electrolyte containing PVP dissolved ethanol media has PVP and ethoxy groups on their surfaces, as shown in Fig. 1b.

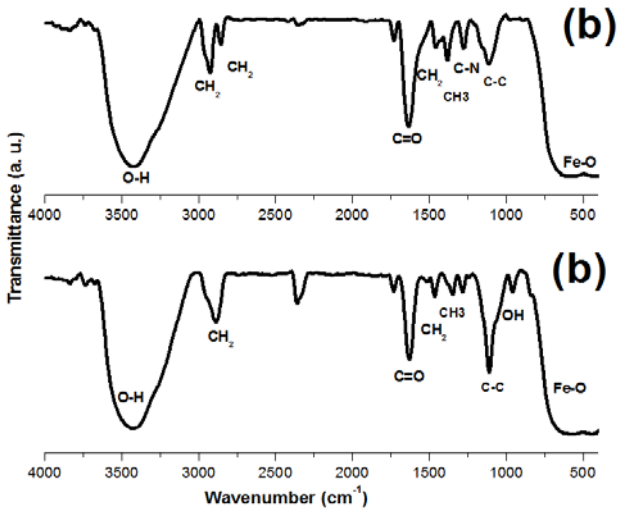

Fig. 3. IR spectra of (a) the pristine and (b) the PVP-grafted Fe_3O_4 NPs

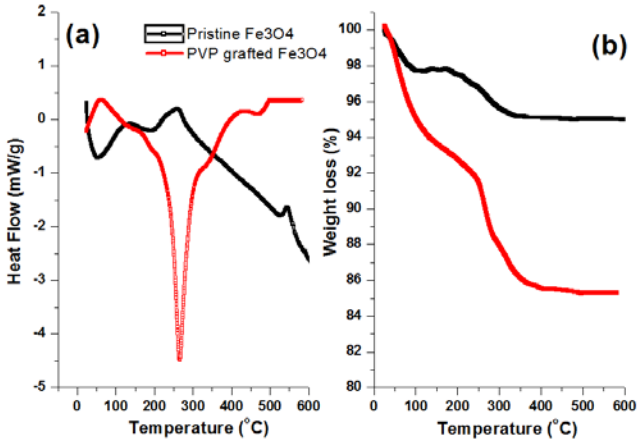

Fig. 4. Thermogravimetric behavior of the prepared SPNs; (a) DSC and (b) the related TG curves

The DSC and related TG curves of the prepared samples are presented in Fig. 4. Two endothermic peaks located in the DSC profile of the pristine Fe_3O_4 (Fig. 4a) are relating to

the removal of water and hydroxyl groups attached on the Fe_3O_4 surface and removal of ethoxy groups connected into Fe_3O_4 surface, respectively. For these two peaks, TG profile of pristine Fe_3O_4 exhibited 2.01% and 7.2% weight losses, respectively. After these steps, no weigh loss on TG profile of pristine Fe_3O_4 is observed up to 600 °C. Notably, one exothermic peak at about 550 ^oC is only presented corresponding to the magnetite phase conversion into hematite [31,55]. For the pristine Fe_3O_4, a total weight loss of 9.2% is occurred proofing the ethoxy layer on the electrodeposited SPNs, as we reported in previous work [55]. For the PVP-grafted SPNs, DSC and related TG curves are also presented in Fig. 4. these profiles have completely different shapes as compared with those of pristine ones. The DSC profile of the PVP-grafted SPNs present a sharp endothermic peak at about 260oC, which is due to the PVP removal from the surface of magnetite NPs [56-58]. Total weight loss for this sample is about 15.6%. This weight loss confirmed the presence of PVP onto the surface of electrodeposited SPNs.

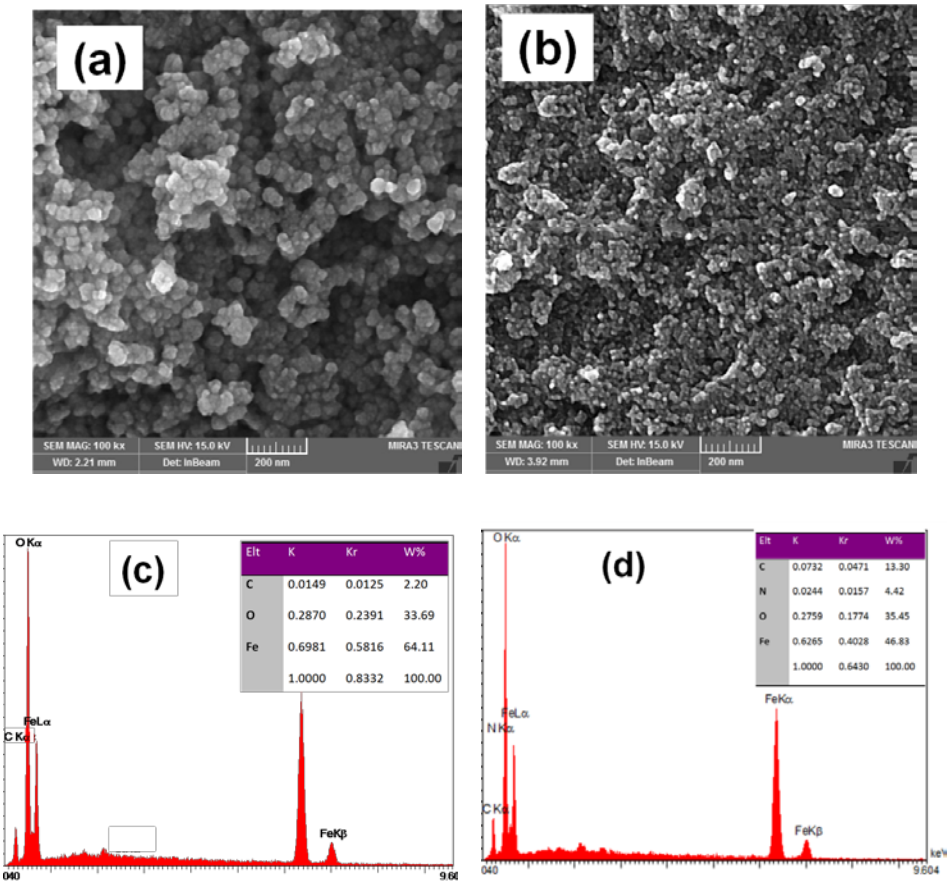

Fig. 5. FE-SEM images and EDS data for (a,c) the pristine and (b,d) PVP grafted Fe_3O_4 samples

The surface morphology of the fabricated pristine and PVP-grafted Fe_3O_4 nanoparticles are given in Figs. 5a and b. For both samples, well-defined particle morphology is clearly

observable. The PVP-grafted Fe_3O_4 sample has better particle-shape and smaller particles size as compare with that of uncoated Fe_3O_4 sample (Fig. 5b). In fact, the pristine Fe_3O_4 particles are rather a agglomerated as compared with the PVP-grated NPs (Fig. 5a). The particle sizes of pristine and PVP-grafted Fe_3O_4 nanoparticles were observed to be ~15 nm and ~10 nm respectively. These observations indicated that the size of electro-synthesized magnetite particles is reduced at the presence of PVP as additive. This result my come from the PVP role in the formation and deposit growth like as surface stabilizer, growth modifier, nanoparticle dispersant, and reducing agent [62]. The hydrodynamic diameters of the prepared SPNs are shown in Fig. 6, which have been measured through a DLS particle size analyzer. It was obtained that the pristine and PVP-grated SPNs have the mean hydrodynamic diameters of 36nm and 78 nm, respectively (Figs. 6a and b). This size increase completely proved the grafting of SPNs by PVP polymer.

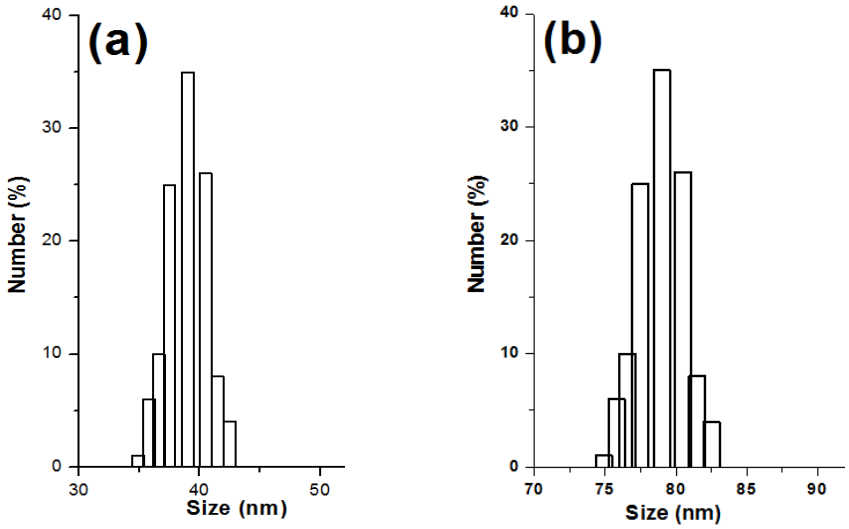

Fig. 6. Hydrodynamic diameter distribution (a) the pristine and (b) PVP-grafted Fe_3O_4 NPs

Fig. 7 exhibits the magnetization curves of the both prepared SPNs, the measured magnetic values are presented in Table 1. This is evidence that both samples have superparamagnetic nature at room temperature, with no hysteresis and a perfect Langevin behavior. The saturation magnetization (*Ms*) values of the pristine and PVP-grafted Fe_3O_4 nanoparticles were measured to be 44.84 and 48.58 emu g^{-1}, respectively, confirming their superparamagnetic nature. This result confirms the increasing the saturation magnetization of Fe_3O_4 nanoparticles with deposition at the presence of PVP. Furthermore, the remaining magnetization (Mr) and coercivity (C_e) were measured to be; $Mr \approx 0.123$ emu g^{-1} and $Ce \sim 4.81G$ for the pristine Fe_3O_4 nanoparticles, and $Mr \approx 0.038$ emu g^{-1} and $Ce \sim 1.23G$ for the PVP-grafted Fe_3O_4 nanoparticles, as noted in Table 1. These values indicated that PVP-

grafted Fe_3O_4 nanoparticles are capable to exhibit very negligible *Mr* and *Ce* values, which indicated their better magnetic behavior as compared to the pristine Fe_3O_4 nanoparticles.

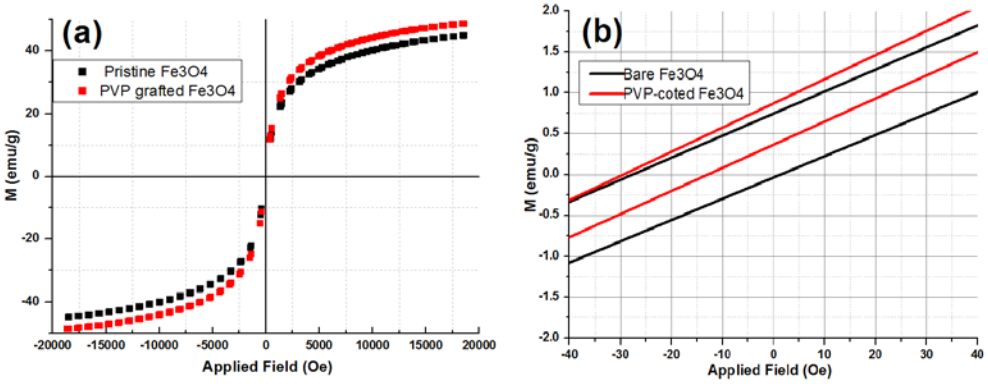

Fig. 7. (a) Hysteresis curves of the pristine and PVP grafted Fe_3O_4 nanoparticles and (b) hysterises at low magnefic field

Table 1. Magnetic data obtained from VSM measurements

Sample name	Ms(emu/g)	Negative Mr(emu/g)	Positive Mr(emu/g)	Retentivity (emu/g)	Negative Hci(G)	Positive Hci (G)	Coercivity (G)
Pristine Fe_3O_4[53]	44.838	-0.036	0.211	0.123	-8.22	1.384	4.81
PVP grafted Fe_3O_4	48.578	0.367	0.289	0.038	-12.96	-10.25	1.35

4. CONCLUSION

In this work, the constant current (CC) electrodeposition of Fe_3O_4 nanoparticles were carried out at the presence of PVP polymer (as an additive and grafting agent) from ethanol (96%) electrolyte. The electrochemical formation of Fe_3O_4 nanoparticles were confirmed by various analyses of XRD, IR, FE-SEM and TGA. The grafting of Fe_3O_4 nanoparticles by PVP layer was confirmed by DLS and TG results. The obtained results indicated that the fabrication of Fe_3O_4 nanoparticles in both pristine and polymer-grafted forms could be achieved through cathodic deposition from Fe(III) nitrate solution with PVP additive.

REFERENCES

[1] J. Gupta, A. Prakash, M. K. Jaiswal, A. Agarrwa, and D. Bahadur, J. Magn. Magn. Mater. 448 (2018) 332.

[2] L. Gholami, R. Kazemi Oskuee, M. Tafaghodi, A. Ramezani Farkhani, and M. Darroudi Ceram. Int. (2018) In Press.
[3] S. Trabulo, A. Aires, A. Aichera, C. Heeschen, and A. L. Cortajaren, Biochim. Biophys. Acta 1861 (2017) 1597.
[4] N. Alegret, A. Criado, and M. Prato, Curr. Med. Chem. 24 (2017) 529.
[5] Wahajuddin, and S. Arora, Int. J. Nanomed. 7 (2012) 3445.
[6] O. Karaagac, and H. Kockar, J. Superconduct. Novel Magn. 25 (2012) 2777.
[7] A. B. Salunkhe, V. M. Khot, J. M. Ruso, and S. I. Patil, RSC Adv. 5 (2015) 18420.
[8] H. Iida, T. Nakanishi, H. Takada, and T. Osaka, Electrochim. Acta 52 (2006) 292.
[9] S. F. Hasany, I. Ahmed, J. Rajan, and A. Rehman, Nanosci. Nanotechnol. 2 (2012) 148.
[10] M. Aghazadeh, and M. R. Ganjali, J. Mater. Sci. 53 (2018) 295.
[11] M. Aghazadeh, and M. R. Ganjali, J. Mater. Sci.: Mater. Electron.29 (2018) 2291.
[12] M. Aghazadeh, and M. R. Ganjali, Ceram. Int. 44 (2018) 520.
[13] M. Bellusci, C. Aliotta, D. Fiorani, A. La Barbera, F. Padella, D. Peddis, M. Pilloni, D. Secci, J. Nanopart. Res. 14 (2012) 904.
[14] M. Bouchard, M. Létourneau, C. Sarra-Bournet, M. Laprise-Pelletier, S. Turgeon, P. Chevallier, J. Lagueux, G. Laroche, and M. A. Fortin, Langmuir 14 (2015) 7633.
[15] A. Ali, H. Zafar, M. Zia, I. ulHaq, A. RehmanPhull, J.S. Ali, and A. Hussain, Nanotechnol. Sci. Appl. 9 (2016) 49.
[16] S. Chaitoglou, M. Reza Sanaee, N. Aguil´o-Aguayo, and E. Bertran, J. Nanomater. 2014 (2014) 178524.
[17] R. Strobel, and S. E. Pratsinis, Adv. Powder Technol. 20 (2009) 190.
[18] G. Martınez, A. Malumbres, R. Mallada, J.L. Hueso, S. Irusta, O. Bomat-Miguel, and J. Santamarıa, Nanotechnology 23 (2012) 425605.
[19] S. Laurent, and M. Mahmoudi, Int. J. Mol. Epidemiol. 2 (2011) 367.
[20] R. Hufschmid, H. Arami, R. M. Ferguson, M. Gonzales, E. Teeman, L. N. Brush, N. D. Browning, and K. M. Krishnan, Nanoscale 7 (2015) 11142.
[21] M. Unni, A. M. Uhl, S. Savliwala, B. H. Savitzky, R. Dhavalikar, N. Garraud, D. P. Arnold, L. F. Kourkoutis, J. S. Andrew, and C. Rinaldi, ACS Nano 11 (2017) 2284.
[22] S. Ge, X. Shi, K. Sun, C. Li, C. Uher, J. R. Baker, M. M. BanaszakHoll, and B. G. Orr, J. Phys. Chem. C 113 (2009) 13593.
[23] H. Cai, X. An, J. Cui, J. Li, S. Wen, K. Li, M. Shen, L. Zheng, G. Zhang, and X. Shi, ACS Appl. Mater. Interfaces 5 (2013) 1722.
[24] D. MishraRuma, A. Swati, L. Sudhir, S. Amritphale, and N. Chandra, Prot. Met. Phys. Chemi. Surf.50 (2014) 628.
[25] Z. Kozakova, I. Kuritka, N. E. Kazantseva, V. Babayan, M. Pastorek, M. Machovsky, P. Bazant, and P. Saha, Dalton Trans. 44 (2015) 21099.
[26] K. Deshpande, A. Mukasyan, and A. Varma, Chem. Mater. 16 (2004) 4896.

[27] R. Ianoş, A. Taculescu, C. Pacurariu, and I. Lazau, J. Am. Ceram. Soc. 95 (2012) 2236.
[28] M. Aghazadeh, P. Kolivand, I. Karimzadeh, M. R. Ganjali, and D. Gharailou, Curr. Nanosci.13 (2017) 274.
[29] I. Karimzadeh, M. Aghazadeh, T. Doroudi, M. R. Ganjali, and D. Gharailou, J. Cluster Sci. 28 (2017) 1259.
[30] I. Karimzadeh, M. Aghazadeh, M. R. Ganjali, P. Norouzi, and T. Doroudi, Mater. Lett. 189 (2017) 290.
[31] I. Karimzadeh, M. Aghazadeh, M. R. Ganjali, and T. Dourudi, Curr. Nanosci. 13 (2017) 167.
[32] I. Karimzadeh, H. Rezagholipour Dizaji, and M. Aghazadeh, Mater. Res. Express 3 (2016) 095022.
[33] H. M. Shiri, and M. Aghazadeh, J. Electrochem. Soc. 159 (2012) E132.
[34] M. Aghazadeh, A. N. Golikand, M. Ghaemi, and T. Yousefi, Mater. Lett. 65 (2011) 1466.
[35] J. Talat Mehrabad, M. Aghazadeh, M. Ghannadi Maragheh, M. R. Ganjali, Mater. Lett. 184 (2016) 223.
[36] M. Aghazadeh, M. R. Ganjali, and P. Norouzi, J. Mater. Sci.: Mater. Electron.27 (2016) 7707.
[37] M. Aghazadeh, M. Ghaemi, A. N. Golikand, and A. Ahmadi, Mater. Lett. 65 (2011) 2545.
[38] M. Aghazadeh, B. Sabour, M. R. Ganjali, and S. Dalvand, Appl. Surf. Sci. 313 (2014) 581.
[39] M. Aghazadeh, M. Hosseinifard, B. Sabour, and S. Dalvand, Appl. Surf. Sci. 287 (2013) 187.
[40] J. Tizfahm, B. Safibonab, M. Aghazadeh, A. Majdabadi, and B. Sabour, Colloids Surf. A 443 (2014) 544.
[41] M. Aghazadeh, and S. Dalvand, J. Electrochem. Soc. 161 (2014) D18.
[42] M. Aghazadeh, R. Ahmadi, D. Gharailou, M.R. Ganjali, and P. Norouzi, J. Mater. Sci.: Mater. Electron. 27 (2017) 8623.
[43] M. Aghazadeh, T. Yousefi, and M. Ghaemi, J. Rare Earths 30 (2012) 236.
[44] M. Aghazadeh, M. G. Maragheh, M. R. Ganjali, and P. Norouzi, RSC Adv. 6 (2016) 10442.
[45] F. Fajaroh, H. Setyawan, W. Widiyastuti, S. Winardi, Adv. Powder. Technol. 23 (2012) 328.
[46] D. Ramimoghadam, S. Bagheri, and S. B. Abd Hamid, J. Magn. Magn.Mater.368 (2014) 207.
[47] S. Franger, P. Berthet, and J. Berthon, J. Solid State Electrochem. 8 (2004) 218.

[48] N. Salamun, H. X. Ni, S. Triwahyono, A. Abdul Jalil, and A. Hakimah Karim, J. Fundamental Sci. 7 (2011) 89.
[49] L. Cabrera, S. Gutierrez, N. Menendez, M. P. Morales, and P. Herrasti, Electrochim. Acta 53 (2008) 3436.
[50] H. M. Kothari, E. A. Kulp, S. J. Limmer, P. Poizot, E. W. Bohannan, and J. A. Switzer, J. Mater. Res. 21 (2006) 293.
[51] R. F. C. Marques, C. Garcia, P. Lecante, S. J. L. Ribeiro, L. Noe, N. J. O. Silva, V. S. Amaral, A. Millan, and M. Verelst, J. Magn. Magn. Mater. 320 (2008) 2311.
[52] M. Ibrahim, K. G. Serrano, L. Noea, C. Garcia, and M. Verelst, Electrochim. Acta 55 (2009) 155.
[53] M. Aghazadeh, Mater. Lett. 211 (2018) 225.
[54] M. Aghazadeh, M. R. Ganjali, and P. Noruzi, Thin Solid Films 634 (2017) 24.
[55] M. Aghazadeh, I. Karimzadeh, M. R. Ganjali, and A. Behzad, J. Mater. Sci.: Mater. Electron. 28 (2017) 18121.
[56] M. Aghazadeh, I. Karimzadeh, and M. R. Ganjali, J. Mater. Sci.: Mater. Electron. 28 (2017) 19061.
[57] H. Y. Lee, N. H. Lim, J. A. Seo, S. H. Yuk, B. K. Kwak, and G. Khang, J. Biomed. Mater. Res. 79B (2006) 142.
[58] Y. Zhang, J. Y. Liu, S. Ma, Y. J. Zhang, X. Zhao, X. D. Zhang, and Z. D. Zhang, J. Mater. Sci.: Mater. Med. 21 (2010) 1205.
[59] H. Y. Lee, S. H. Lee, C. Xu, J. Xie, J. H. Lee, B. Wu, A. L. Koh, and X. Wang, Nanotechnol. 19 (2008) 165101.
[60] I. Karimzadeh, M. Aghazadeh, M. R. Ganjali, P. Norouzi, and S. Shirvani-Arani, Mater. Lett. 179 (2016) 5.
[61] X. Lu, M. Niu, R. Qiao, and M. Gao, J. Phys. Chem. B 112 (2008) 14390.
[62] M. Aghazadeh, and I. Karimzadeh, Curr. Nanosci. 14 (2018) 42.
[63] K. M. Koczkur, S. Mourdikoudis, L. Polavarapu, and S. E. Skrabalak, Dalton Trans. 44 (2015) 17883.